

19. COSMIC BACKGROUND RADIATION

Revised February 2000 by G.F. Smoot (LBNL) and D. Scott (University of British Columbia).

19.1. Introduction

The observed cosmic microwave background (CMB) radiation provides strong evidence for the hot big bang. The success of primordial nucleosynthesis calculations (see Sec. 16, “Big-bang nucleosynthesis”) requires a cosmic background radiation (CBR) characterized by a temperature $kT \sim 1$ MeV at a redshift of $z \simeq 10^9$. In their pioneering work, Gamow, Alpher, and Herman [1] realized this and predicted the existence of a faint residual relic, primordial radiation, with a present temperature of a few degrees. The observed CMB is interpreted as the current manifestation of the required CBR.

The CMB was serendipitously discovered by Penzias and Wilson [2] in 1965. Its spectrum is well characterized by a 2.73 K black-body (Planckian) spectrum over more than three decades in frequency (see Fig. 19.1). A non-interacting Planckian distribution of temperature T_i at redshift z_i transforms with the universal expansion to another Planckian distribution at redshift z_f with temperature $T_f/(1+z_f) = T_i/(1+z_i)$. Hence thermal equilibrium, once established (*e.g.* at the nucleosynthesis epoch), is preserved by the expansion, in spite of the fact that photons decoupled from matter at early times. Because there are about 10^9 photons per nucleon, the transition from the ionized primordial plasma to neutral atoms at $z \sim 1000$ does not significantly alter the CBR spectrum [3].

19.2. The CMB frequency spectrum

The remarkable precision with which the CMB spectrum is fitted by a Planckian distribution provides limits on possible energy releases in the early Universe, at roughly the fractional level of 10^{-4} of the CBR energy, for redshifts $\lesssim 10^7$ (corresponding to epochs $\gtrsim 1$ year). The following three important classes of theoretical spectral distortions (see Fig. 19.2) generally correspond to energy releases at different epochs. The distortion results from the CBR photon interactions with a hot electron gas at temperature T_e .

19.2.1. Compton distortion: Late energy release ($z \lesssim 10^5$). Compton scattering ($\gamma e \rightarrow \gamma' e'$) of the CBR photons by a hot electron gas creates spectral distortions by transferring energy from the electrons to the photons. Compton scattering cannot achieve thermal equilibrium for $y \lesssim 1$, where

$$y = \int_0^z \frac{kT_e(z') - kT_\gamma(z')}{m_e c^2} \sigma_T n_e(z') c \frac{dt}{dz'} dz' , \quad (19.1)$$

is the integral of the number of interactions, $\sigma_T n_e(z) c dt$, times the mean-fractional photon-energy change per collision [4]. For $T_e \gg T_\gamma$ y is also proportional to the integral of the electron pressure $n_e k T_e$ along the line of sight. For standard thermal histories $y < 1$ for epochs later than $z \simeq 10^5$.

The resulting CMB distortion is a temperature decrement

$$\Delta T_{\text{RJ}} = -2y T_\gamma \quad (19.2)$$

2 19. Cosmic background radiation

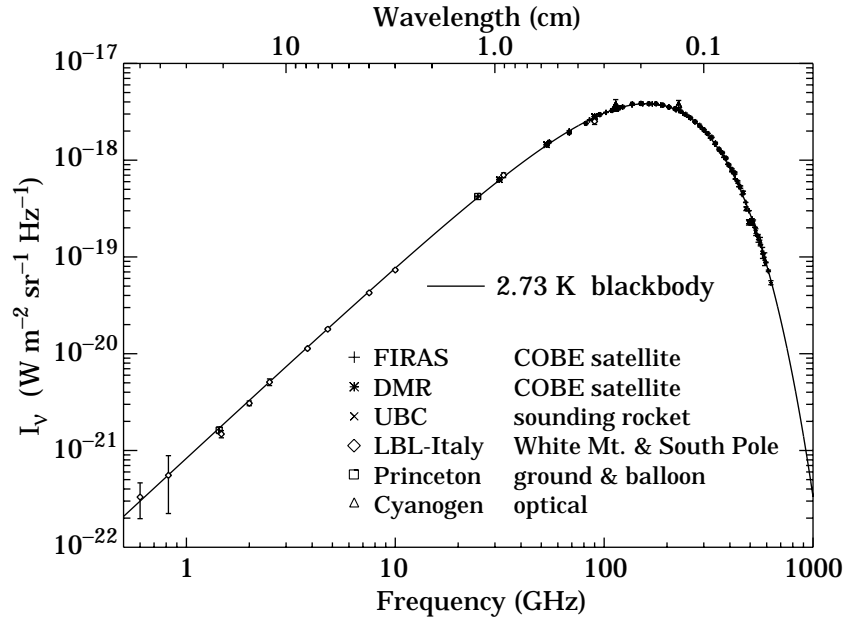


Figure 19.1: Precise measurements of the CMB spectrum. The line represents a 2.73 K blackbody, which describes the spectrum very well, especially around the peak of intensity. The spectrum is less well constrained at 10 cm and longer wavelengths. (References for this figure are at the end of this section under “CMB Spectrum References.”)

in the Rayleigh-Jeans ($h\nu/kT \ll 1$) portion of the spectrum, and a rise in temperature in the Wien ($h\nu/kT \gg 1$) region, *i.e.* photons are shifted from low to high frequencies. The magnitude of the distortion is related to the total energy transfer [4] ΔE by

$$\Delta E/E_{\text{CMB}} = e^{4y} - 1 \simeq 4y . \quad (19.3)$$

A prime candidate for producing a Comptonized spectrum is a hot intergalactic medium. A hot ($T_e > 10^5 \text{ K}$) medium in clusters of galaxies can and does produce a partially Comptonized spectrum as seen through the cluster, known as the Sunyaev-Zel’dovich effect [5]. Based upon X-ray data, the predicted large angular scale total combined effect of the hot intracluster medium should produce $y \sim 10^{-6}$ [6].

19.2.2. Bose-Einstein or chemical potential distortion: Early energy release ($z \sim 10^5\text{--}10^7$). After many Compton scatterings ($y \gg 1$), the photons and electrons will reach statistical (not thermodynamic) equilibrium, because Compton scattering conserves photon number. This equilibrium is described by the Bose-Einstein distribution with non-zero chemical potential:

$$n = \frac{1}{e^{x+\mu_0} - 1} , \quad (19.4)$$

where $x \equiv h\nu/kT$ and $\mu_0 \simeq 1.4 \Delta E/E_{\text{CMB}}$, with μ_0 being the dimensionless chemical potential that is required to conserve photon number.

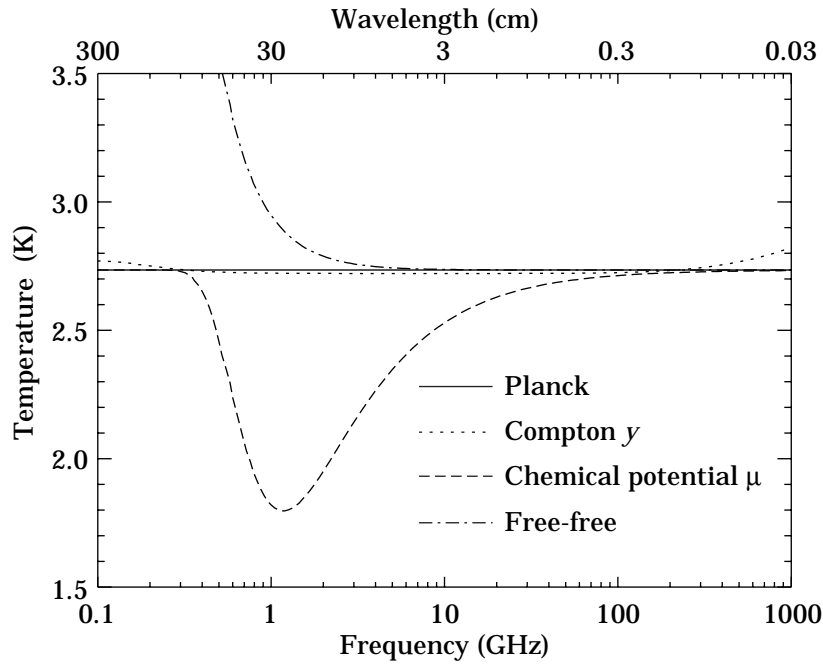


Figure 19.2: The shapes of expected, but so far unobserved, CMB distortions, resulting from energy-releasing processes at different epochs.

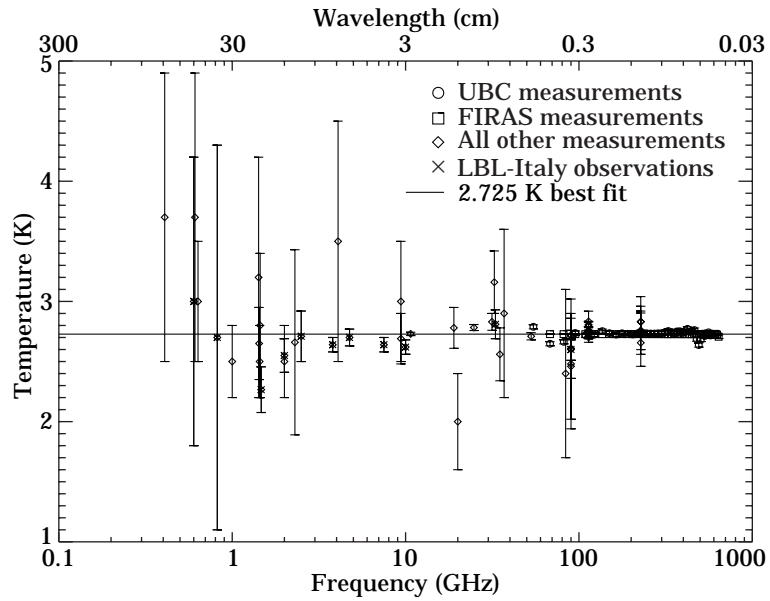


Figure 19.3: Observed thermodynamic temperature as a function frequency.

4 19. Cosmic background radiation

The collisions of electrons with nuclei in the plasma produce free-free (thermal bremsstrahlung) radiation: $eZ \rightarrow e'Z'\gamma$. Free-free emission thermalizes the spectrum to the plasma temperature at long wavelengths and Compton scattering begins to shift these photons upward. Including this effect, the chemical potential becomes frequency-dependent,

$$\mu(x) = \mu_0 e^{-2x_b/x}, \quad (19.5)$$

where x_b is the transition frequency at which Compton scattering of photons to higher frequencies is balanced by free-free creation of new photons. The resulting spectrum has a sharp drop in brightness temperature at centimeter wavelengths [7]. The minimum wavelength is determined by Ω_B .

The equilibrium Bose-Einstein distribution results from the oldest non-equilibrium processes ($10^5 < z < 10^7$), such as the decay of relic particles or primordial inhomogeneities. Note that free-free emission (thermal bremsstrahlung) and radiative-Compton scattering effectively erase any distortions [8] to a Planckian spectrum for epochs earlier than $z \sim 10^7$.

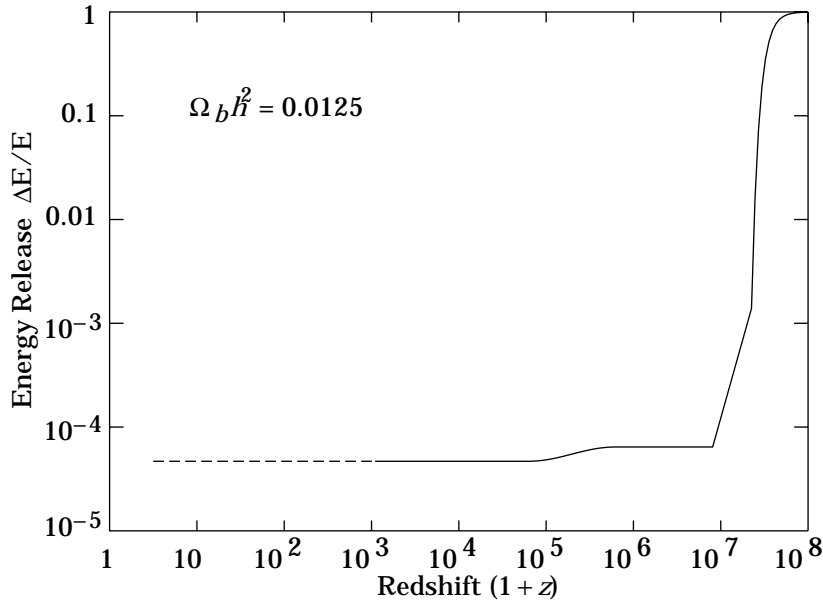


Figure 19.4: Upper Limits (95% CL) on fractional energy ($\Delta E/E_{\text{CMB}}$) releases from processes at different epochs as set by resulting lack of CMB spectral distortions. These can be translated into constraints on the mass, lifetime and photon branching ratio of unstable relic particles, with some additional dependence on cosmological parameters such as Ω_B [11,12].

19.2.3. Free-free distortion: Very late energy release ($z \ll 10^3$). Free-free emission can create rather than erase spectral distortion in the late Universe, for recent reionization ($z < 10^3$) and from a warm intergalactic medium. The distortion arises because of the lack of Comptonization at recent epochs. The effect on the present-day CMB spectrum is described by

$$\Delta T_{\text{ff}} = T_\gamma Y_{\text{ff}}/x^2, \quad (19.6)$$

where T_γ is the undistorted photon temperature, x is the dimensionless frequency, and Y_{ff}/x^2 is the optical depth to free-free emission:

$$Y_{\text{ff}} = \int_0^z \frac{T_e(z') - T_\gamma(z')}{T_e(z')} \frac{8\pi e^6 h^2 n_e^2 g}{3m_e (kT_\gamma)^3 \sqrt{6\pi} m_e kT_e} \frac{dt}{dz'} dz'. \quad (19.7)$$

Here h is Planck's constant, n_e is the electron density and g is the Gaunt factor [9].

19.2.4. Spectrum summary: The CMB spectrum is consistent with a blackbody distribution over more than three decades of frequency around the peak. The best-fit to the COBE FIRAS data yields $T_\gamma = 2.725 \pm 0.002$ K (95% CL) [10]. The following table is a summary of all CMB spectrum measurements:

$$\begin{aligned} T_\gamma &= 2.725 \pm 0.002 \text{ K} \quad (95\% \text{ CL}); \\ n_\gamma &= (2\zeta(3)/\pi^2) T_\gamma^3 \simeq 411 \text{ cm}^{-3}; \\ \rho_\gamma &= (\pi^2/15) T_\gamma^4 \simeq 4.64 \times 10^{-34} \text{ g cm}^{-3} \simeq 0.260 \text{ eV cm}^{-3}; \\ |y| &< 1.2 \times 10^{-5} \quad (95\% \text{ CL}); \\ |\mu_0| &< 9 \times 10^{-5} \quad (95\% \text{ CL}); \\ |Y_{\text{ff}}| &< 1.9 \times 10^{-5} \quad (95\% \text{ CL}). \end{aligned}$$

These limits [13] correspond to constraints [13–15] on energetic processes $\Delta E/E_{\text{CMB}} < 2 \times 10^{-4}$ occurring between redshifts 10^3 and 5×10^6 (see Fig. 19.4).

19.3. Deviations from isotropy

Penzias and Wilson reported that the CMB was isotropic and unpolarized at the 10% level. Current observations show that the CMB is unpolarized at the 10^{-5} level but has a dipole anisotropy at the 10^{-3} level, with smaller-scale anisotropies at the 10^{-5} level. Standard theories predict temperature anisotropies of roughly the amplitude now being detected, and anisotropies in linear polarization at a level which should soon be reached.

It is customary to express the CMB temperature anisotropies on the sky in a spherical harmonic expansion,

$$\frac{\Delta T}{T}(\theta, \phi) = \sum_{\ell m} a_{\ell m} Y_{\ell m}(\theta, \phi), \quad (19.8)$$

and to discuss the various multipole amplitudes. The power at a given angular scale is roughly $\ell \sum_m |a_{\ell m}|^2 / 4\pi$, with $\ell \sim 1/\theta$.

6 19. Cosmic background radiation

19.3.1. The dipole: The largest anisotropy is in the $\ell = 1$ (dipole) first spherical harmonic, with amplitude at the level of $\Delta T/T = 1.23 \times 10^{-3}$. The dipole is interpreted as the result of the Doppler shift caused by the solar system motion relative to the nearly isotropic blackbody field, as confirmed by measurements of the velocity field of local galaxies [16]. The motion of the observer (receiver) with velocity $\beta = v/c$ relative to an isotropic Planckian radiation field of temperature T_0 produces a Doppler-shifted temperature

$$\begin{aligned} T(\theta) &= T_0(1 - \beta^2)^{1/2}/(1 - \beta \cos \theta) \\ &= T_0 \left(1 + \beta \cos \theta + (\beta^2/2) \cos 2\theta + O(\beta^3) \right) . \end{aligned} \quad (19.9)$$

The implied velocity [13,17] for the solar-system barycenter is $\beta = 0.001237 \pm 0.000002$ (68% CL) or $v = 371 \pm 0.5 \text{ km s}^{-1}$, assuming a value $T_0 = T_\gamma$, towards $(\alpha, \delta) = (11.20^{\text{h}} \pm 0.01^{\text{h}}, -7.22^\circ \pm 0.08^\circ)$, or $(\ell, b) = (264.31^\circ \pm 0.17^\circ, 48.05^\circ \pm 0.10^\circ)$. Such a solar-system velocity implies a velocity for the Galaxy and the Local Group of galaxies relative to the CMB. The derived velocity is $v_{\text{LG}} = 627 \pm 22 \text{ km s}^{-1}$ toward $(\ell, b) = (276^\circ \pm 3^\circ, 30^\circ \pm 3^\circ)$, where most of the error comes from uncertainty in the velocity of the solar system relative to the Local Group.

The Doppler effect of this velocity and of the velocity of the Earth around the Sun, as well as any velocity of the receiver relative to the Earth, is normally removed for the purposes of CMB anisotropy study. The resulting high degree of CMB isotropy is the strongest evidence for the validity of the Robertson-Walker metric.

19.3.2. The quadrupole: The rms quadrupole anisotropy amplitude is defined through $Q_{\text{rms}}^2/T_\gamma^2 = \sum_m |a_{2m}|^2/4\pi$. The current estimate of its value is $4 \mu\text{K} \leq Q_{\text{rms}} \leq 28 \mu\text{K}$ for a 95% confidence interval [18]. The uncertainty here includes both statistical errors and systematic errors, which are dominated by the effects of galactic emission modelling. This level of quadrupole anisotropy allows one to set general limits on anisotropic expansion, shear, and vorticity; all such dimensionless quantities are constrained to be less than about 10^{-5} .

For specific homogeneous cosmologies, fits to the whole anisotropy pattern allow stringent limits to be placed on, for example, the global rotation at the level of about 10^{-7} of the expansion rate [19].

19.3.3. Smaller angular scales: The COBE-discovered [20] higher-order ($\ell > 2$) anisotropy is interpreted as being the result of perturbations in the energy density of the early Universe, manifesting themselves at the epoch of the CMB's last scattering. The detection of these anisotropies at just the right level for gravity to have grown all of the structure observed in today's Universe demonstrates that gravitational instability acting on primordial density perturbations was the main mechanism for structure formation.

Theoretical models generally predict a power spectrum in spherical harmonic amplitudes, since the models lead to primordial fluctuations and thus $a_{\ell m}$ that are Gaussian random fields, and hence the power spectrum in ℓ is sufficient to characterize the results. The power at each ℓ is $(2\ell + 1)C_\ell/(4\pi)$, where $C_\ell \equiv \langle |a_{\ell m}|^2 \rangle$ and a statistically isotropic sky means that all m 's are equivalent. For an idealized full-sky observation, the

variance of each measured C_ℓ is $[2/(2\ell + 1)]C_\ell^2$. This sampling variance (known as cosmic variance) comes about because each C_ℓ is chi-squared distributed with $(2\ell + 1)$ degrees of freedom for our observable volume of the Universe [21].

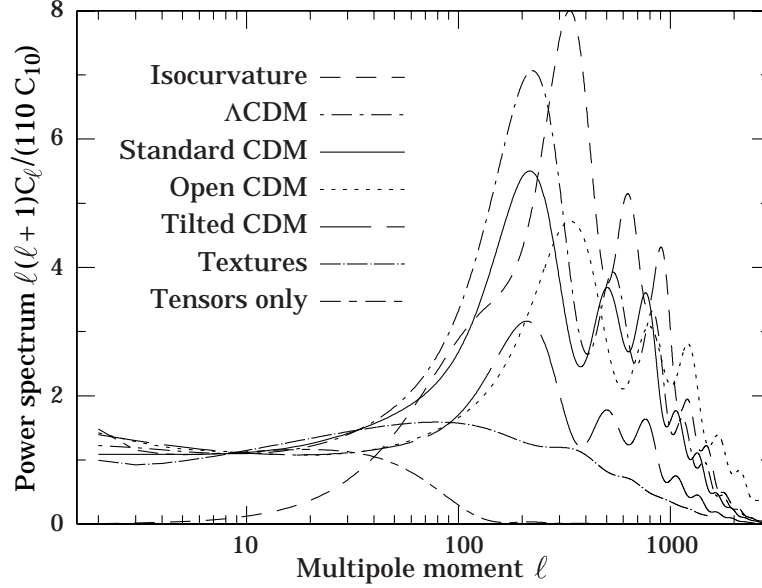


Figure 19.5: Theoretically predicted $\ell(\ell + 1)C_\ell$ or CMB anisotropy power spectra [24] for a range of models. The top curve is an isocurvature CDM model which has a characteristically different shape than the adiabatic models. The next four are variants of adiabatic Cold Dark Matter models. The textures model [25] is an example with perturbations seeded by topological defects. We also show the power spectrum from gravity waves (tensors), which could contribute at large angles. All the models have been normalized at $\ell = 10$ except for the isocurvature case, which was arbitrarily normalized to the height of the box. Such curves depend in detail on the precise values of the cosmological parameters, and those shown here are examples only.

Figure 19.5 shows the theoretically predicted anisotropy power spectrum for a sample of models, plotted as $\ell(\ell + 1)C_\ell$ versus ℓ which is the power per logarithmic interval in ℓ or, equivalently, the two-dimensional power spectrum. If the initial power spectrum of perturbations is the result of quantum mechanical fluctuations produced and amplified during inflation, then for simple models the shape of the anisotropy spectrum is coupled to the ratio of contributions from density (scalar) and gravitational wave (tensor) perturbations [22]. In such models the large angle contribution from tensors is constrained to be $\lesssim 0.5$ [23]. However, there are other inflationary models which allow higher tensor contribution. In particular if the energy scale of inflation at the appropriate epoch is $\simeq 10^{16}\text{GeV}$, then detection of the effect of gravitons is more likely and partial reconstruction of the inflaton potential may be feasible. However, if the energy scale is $\lesssim 10^{14}\text{GeV}$, then typically density fluctuations dominate and less constraint is possible.

8 19. Cosmic background radiation

On angular scales corresponding to $\ell \gtrsim 50$ scalar modes certainly dominate. In the standard scenario the last scattering epoch happens at a redshift of approximately 1100, by which time the large number of photons was no longer able to keep the hydrogen ionized. The optical thickness of the cosmic photosphere is roughly $\Delta z \sim 100$ corresponding to about 5 arcminutes on the sky, so that features smaller than this size are damped.

Anisotropies have now been observed on angular scales above this damping scale by a large number of experiments (see Fig. 19.6), and are consistent with those expected from an initially scale-invariant (also referred to as ‘flat’) power spectrum of potential and thus metric fluctuations. The initial spectrum of density perturbations is reflected in the large angle (small ℓ) power spectrum, but perturbations can evolve significantly in the epoch $z \gtrsim 1100$ for causally connected regions (angles $\lesssim 1^\circ \Omega_{\text{tot}}^{1/2}$). The primary mode of evolution is through acoustic oscillations, leading to a series of peaks at small angular scales, which encode information about the primordial perturbations, geometry, matter and radiation content, and ionization history of the Universe [26]. Thus, precise measurement of the shape of the anisotropy power spectrum will provide information on the amplitude and slope of the initial conditions, as well as Ω_0 , Ω_B , Ω_Λ (cosmological constant), H_0 and other cosmological parameters.

Fits to experimental data are often quoted as the expected value of the quadrupole $\langle Q \rangle$ for some specific theory over some range of ℓ (*e.g.* a model with power-law initial conditions, having primordial density perturbation power spectrum $|\delta_k|^2 \propto k^n$). The full 4-year COBE DMR data give $\langle Q \rangle = 15.3_{-2.8}^{+3.7} \mu\text{K}$, after projecting out the slope dependence, while the best-fit slope is $n = 1.2 \pm 0.3$, and for a pure $n = 1$ (scale-invariant potential perturbation) spectrum $\langle Q \rangle (n = 1) = 18 \pm 1.6 \mu\text{K}$ [18,27]. The conventional notation is such that $\langle Q \rangle^2 / T_\gamma^2 = 5C_2 / 4\pi$. An alternative convention is to quote the ‘band-power’ $\sqrt{\ell(2\ell + 1)C_\ell / 4\pi}$. Many recent experiments give results for a number of band-powers covering different ranges of ℓ . $\langle Q \rangle^2 / T_\gamma^2 = 5C_2 / 4\pi$. fluctuations measured by other experiments can also be quoted in terms ($n = 1$)

The initial density perturbations can either be ‘adiabatic’ (meaning that there is no change to the entropy per particle for each species) or ‘isocurvature’ (meaning that, for example, matter perturbations compensate radiation perturbations so that the total energy density remains unchanged). Within the family of adiabatic models, the location of the first acoustic peak is predicted to be at $\ell \sim 220 \Omega_{\text{tot}}^{-1/2}$ or $\theta \sim 0.3^\circ \Omega_{\text{tot}}^{1/2}$ and its amplitude is a calculable function of the parameters (see Fig. 19.5).

It has been clear for several years that there is more power at sub-degree scales than at COBE scales [26]. More recently results have indicated that there is a localized peak, and the general shape of the power spectrum favors adiabatic-type perturbations (compare Fig. 19.5 and Fig. 19.6). Within the adiabatic scenario, the currently available data imply that the Universe is close to flat [28], with $0.62 < \Omega_{\text{tot}} < 1.24$ (95% CL) [29]. Together with a number of observations indicating that the matter density $\Omega_M \simeq 0.3$ (*e.g.* see Ref. 37), this implies that there is some unknown contribution to the energy, ‘dark energy,’ which is independently indicated through distant supernova studies [30]. The height of the peak can also be used to constrain models, but currently the results depend sensitively on what range of models are considered and what other cosmological

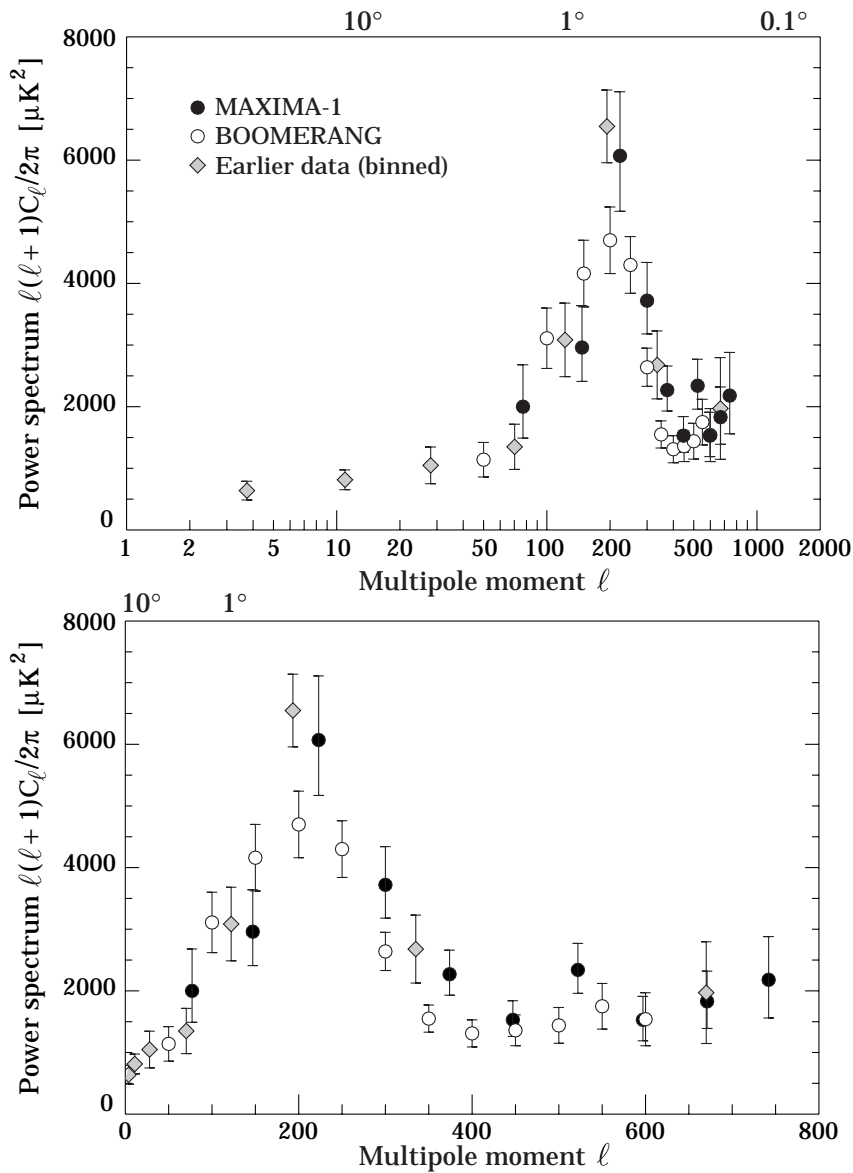


Figure 19.6: There is now so much CMB data that it is difficult and confusing to show all the individual results. Instead the figure shows the new BOOMERANG [32] (open circles) and MAXIMA [33] data (filled circles), together with binned results of all previous experiments, based on data with references given at the end of this section under “CMB Anisotropy References.” The previous data are shown as grey diamonds, which were obtained [38] by maximizing the likelihood for a power spectrum assumed to be piece-wise constant between $\ell = 2$ and 1000, permitting experimental errors to be asymmetric, and allowing for correlated (continued) ...

10 19. Cosmic background radiation

Figure 19.6: (continued) calibration uncertainties for each experiment [39]. These binned values are somewhat correlated, partly explaining the apparent discrepancy, which is consistent with calibration uncertainties between experiments. The sub-set of data from the first Antarctic flight of BOOMERANG and the data from the MAXIMA-1 flight are independent, with essentially no correlations between bins. The figure clearly shows a localized peak at $\ell \simeq 200$ and some structure at higher ℓ . Upper limits at smaller angular scales, indicating further evidence for a falloff at high ℓ , have not been shown.

constraints are used [28,29,31]. Detailed measurements of parameters are expected to follow soon, but certainly some more general questions are already being answered.

Recent experimental results from the Boomerang 98 [32] and MAXIMA-1 [33] balloon flights have dramatically improved the power spectrum measurements. These new data indicate a very well-defined first acoustic peak, at close to the position expected in flat models with adiabatic fluctuations. It is difficult generate this feature by an incoherent causal mechanism, such as with topological defects. The position of the first peak constrains the total density parameter to be $\Omega_{\text{tot}} \simeq 1.0 \pm 0.1$ [34,35]. Intriguingly, the second peak does not appear as pronounced as had been expected in the previously favored models. There are several ways to explain this [36], including a combination of tilt, higher baryon density and some other mild parameter variations, as well as more exotic explanations such as delayed recombination, partial loss of coherence of the oscillations, or features in the underlying power spectrum. Detailed measurement of the second and third peaks ought to distinguish among these possibilities.

Causal mechanisms, such as arise in topological defect models, cannot naturally account for the observed power spectrum (see Fig. 19.5), and isocurvature models also generically give the wrong shape. Thus the present data appear to point to models with adiabatic and apparently acausal fluctuations. Since inflation is the only mechanism we have to provide the large-scale homogeneity and anisotropy observed in the universe and to produce these apparently acausal fluctuations, one might consider the current CMB data as supporting the inflationary paradigm. A more stringent test of inflation will be provided with the arrival of data that have the fidelity to resolve the sub-degree region into the oscillating peaks and troughs which must be present in inflationary models.

New data are being acquired at an increasing rate, with a large number of improved ground- and balloon-based experiments being developed. The current suite of experiments promises to map out the CMB anisotropy power spectrum to about 10% accuracy, and determine several parameters at the 10 to 20% level in the very near future. A vigorous sub-orbital and interferometric program should push those numbers further in the next few years.

There are also now two approved satellite experiments: the NASA Microwave Anisotropy Probe (MAP), scheduled for launch in late 2000; and the ESA Planck mission, expected to launch in 2007. The improved sensitivity, freedom from earth-based systematics, and all-sky coverage allow a simultaneous determination of many of the cosmological parameters to unprecedented precision: for example, Ω_0 and n to about 1%, Ω_B and H_0 at the level of a few percent [40]. Just as with the frequency spectrum,

precise measurement of the anisotropies should also lead to constraints on a particle physics effects at $z \sim 1000$ [41].

Since Thomson scattering of the anisotropic radiation field also generates linear polarization at the roughly 5% level [42], there is additional cosmological information to be gleaned from polarization measurements. Although difficult to detect, the polarization signal should act as a strong confirmation of the general paradigm. Furthermore, detailed measurement of the polarization signal provides more precise information on the physical parameters. In particular it allows a clear distinction of any gravity wave contribution, which is crucial to probing the $\sim 10^{16}$ GeV energy range. The fulfillment of this promise may await an even more sensitive generation of satellites.

References:

1. R.A. Alpher and R.C. Herman, *Physics Today* **41**, No. 8, p. 24 (1988).
2. A.A. Penzias and R. Wilson, *Astrophys. J.* **142**, 419 (1965);
R.H. Dicke, P.J.E. Peebles, P.G. Roll, and D.T. Wilkinson, *Astrophys. J.* **142**, 414 (1965).
3. P.J.E. Peebles, "Principles of Physical Cosmology," Princeton U. Press, p. 168 (1993).
4. R.A. Sunyaev and Ya.B. Zel'dovich, *Ann. Rev. Astron. Astrophys.* **18**, 537 (1980).
5. M. Birkinshaw, *Phys. Rep.* **310**, 98 (1999).
6. A.C. da Silva, D. Barbosa, A.R. Liddle, and P.A. Thomas, *MNRAS*, in press, astro-ph/9907224.
7. C. Burigana, L. Danese, and G.F. De Zotti, *Astron. & Astrophys.* **246**, 49 (1991).
8. L. Danese and G.F. De Zotti, *Astron. & Astrophys.* **107**, 39 (1982);
G. De Zotti, *Prog. in Part. Nucl. Phys.* **17**, 117 (1987).
9. J.G. Bartlett and A. Stebbins, *Astrophys. J.* **371**, 8 (1991).
10. J.C. Mather *et al.*, *Astrophys. J.* **512**, 511 (1999).
11. E.L. Wright *et al.*, *Astrophys. J.* **420**, 450 (1994).
12. W. Hu and J. Silk, *Phys. Rev. Lett.* **70**, 2661 (1993).
13. D.J. Fixsen *et al.*, *Astrophys. J.* **473**, 576 (1996).
14. J.C. Mather *et al.*, *Astrophys. J.* **420**, 439 (1994).
15. M. Bersanelli *et al.*, *Astrophys. J.* **424**, 517 (1994).
16. A. Dekel, in "Cosmic Flows: Towards an Understanding of Large-Scale Structure", ed. S. Courteau, M.A. Strauss, and J.A. Willick (ASP Conf. Ser.), in press, astro-ph/9911501.
17. A. Kogut *et al.*, *Astrophys. J.* **419**, 1 (1993);
C. Lineweaver *et al.*, *Astrophys. J.* **470**, L28 (1996).
18. C.L. Bennett *et al.*, *Astrophys. J.* **464**, L1 (1996).
19. A. Kogut, G. Hinshaw, and A.J. Banday, *Phys. Rev.* **D55**, 1901 (1997);
E.F. Bunn, P. Ferreira, and J. Silk, *Phys. Rev. Lett.* **77**, 2883 (1996).

12 19. *Cosmic background radiation*

20. G.F. Smoot *et al.*, *Astrophys. J.* **396**, L1 (1992).
21. M. White, D. Scott, and J. Silk, *Ann. Rev. Astron. & Astrophys.* **32**, 329 (1994).
22. D.H. Lyth and A. Riotto, *Phys. Rep.* **314**, 1 (1999).
23. J.P. Zibin, D. Scott, and M. White, *Phys. Rev. D* **60**, 123513 (1999).
24. U. Seljak and M. Zaldarriaga, *Astrophys. J.* **469**, 437 (1996).
25. U.-L. Pen, U. Seljak, and N. Turok, *Phys. Rev. Lett.* **79**, 1611 (1997).
26. D. Scott, J. Silk, and M. White, *Science* **268**, 829 (1995);
W. Hu, J. Silk, and N. Sugiyama, *Nature* **386**, 37 (1996).
27. K.M. Górski *et al.*, *Astrophys. J.* **464**, L11 (1996).
28. S. Dodelson and L. Knox, *Phys. Rev. Lett.*, in press, astro-ph/9909454;
A. Melchiorri *et al.*, *Astrophys. J.*, in press, astro-ph/9911445.
29. M. Tegmark and M. Zaldarriaga, *Astrophys. J.*, in press, astro-ph/0002091.
30. S. Perlmutter *et al.*, *Astrophys. J.* **517**, 565 (1999);
A.G. Riess *et al.*, *Astron. J.* **116**, 1009 (1998).
31. C.H. Lineweaver, *Astrophys. J.* **505**, L69 (1998);
J.R. Bond and A.H. Jaffe, *Phil. Trans. Roy. Soc. A*, in press, astro-ph/98089043;
G. Efstathiou, *MNRAS* **310**, 842 (1999).
32. P. de Bernardis *et al.*, *Nature* **404**, 955 (2000).
33. S. Hanany *et al.*, astro-ph/0005123.
34. A. Lange *et al.*, astro-ph/0005004.
35. A. Balbi *et al.*, astro-ph/0005124.
36. M. White, D. Scott, E. Pierpaoli, astro-ph/0004385.
37. R.G. Carlberg *et al.*, *Astrophys. J.* **462**, 32 (1996);
P. Coles and G.F.R. Ellis, “Is the Universe Open or Closed?”, Cambridge University Press, Cambridge (1997).
38. E. Pierpaoli, D. Scott and M. White, *Science*, in press (2000).
39. J. R. Bond, A.H. Jaffe, and L.E. Knox, *Astrophys. J.*, in press, astro-ph/9808264.
40. G. Jungman, M. Kamionkowski, A. Kosowsky, and D.N. Spergel, *Phys. Rev.* **D54**, 1332 (1996);
W. Hu and M. White, *Phys. Rev. Lett.* **77**, 1687 (1996);
J.R. Bond, G. Efstathiou, and M. Tegmark, *MNRAS* **291**, L33 (1997);
M. Zaldarriaga, D. Spergel, and U. Seljak, *Astrophys. J.* **488**, 1 (1997).
41. M. Kamionkowski, A. Kosowsky, *Ann. Rev. Nucl. Part. Sci.* **49**, 77 (1999).
42. W. Hu, M. White, *New Astron.* **2**, 323 (1997).

CMB Spectrum References:

1. **FIRAS:** J.C. Mather *et al.*, *Astrophys. J.* **420**, 439 (1994);
D. Fixsen *et al.*, *Astrophys. J.* **420**, 445 (1994);

- D. Fixsen *et al.*, *Astrophys. J.* **473**, 576 (1996);
 J.C. Mather *et al.*, *Astrophys. J.* **512**, 511 (1999).
2. **DMR:** A. Kogut *et al.*, *Astrophys. J.* **419**, 1 (1993);
 A. Kogut *et al.*, *Astrophys. J.* **460**, 1 (1996).
 3. **UBC:** H.P. Gush, M. Halpern, and E.H. Wishnow, *Phys. Rev. Lett.* **65**, 537 (1990).
 4. **LBL-Italy:** G.F. Smoot *et al.*, *Phys. Rev. Lett.* **51**, 1099 (1983);
 M. Bensadoun *et al.*, *Astrophys. J.* **409**, 1 (1993);
 M. Bersanelli *et al.*, *Astrophys. J.* **424**, 517 (1994);
 M. Bersanelli *et al.*, *Astrophys. Lett. and Comm.* **32**, 7 (1995);
 G. De Amici *et al.*, *Astrophys. J.* **381**, 341 (1991);
 A. Kogut *et al.*, *Astrophys. J.* **335**, 102 (1990);
 N. Mandolesi *et al.*, *Astrophys. J.* **310**, 561 (1986);
 G. Sironi, G. Bonelli, & M. Limon, *Astrophys. J.* **378**, 550 (1991).
 5. **Princeton:** S. Staggs *et al.*, *Astrophys. J.* **458**, 407 (1995);
 S. Staggs *et al.*, *Astrophys. J.* **473**, L1 (1996);
 D.G. Johnson and D.T. Wilkinson, *Astrophys. J.* **313**, L1 (1987).
 6. **Cyanogen:** K.C. Roth, D.M. Meyer, and I. Hawkins, *Astrophys. J.* **413**, L67 (1993);
 K.C. Roth and D.M. Meyer, *Astrophys. J.* **441**, 129 (1995);
 E. Palazzi *et al.*, *Astrophys. J.* **357**, 14 (1990).

CMB Anisotropy References:

1. **ARGO:** P. de Bernardis *et al.*, *Astrophys. J.* **422**, L33 (1994);
 S. Masi *et al.*, *Astrophys. J.* **463**, L47 (1996).
2. **ATCA:** R. Subrahmayan, M.J. Kesteven, R.D. Ekers, M. Sinclair, and J. Silk,
Monthly Not. Royal Astron. Soc. **298**, 1189 (1993).
3. **BAM:** G.S. Tucker *et al.*, *Astrophys. J.* **475**, L73 (1997).
4. **BOOM97:** P.D. Mauskopf *et al.*, *Astrophys. J.*, in press, astro-ph/9911444.
5. **CAT:** P.F.S. Scott *et al.*, *Astrophys. J.* **461**, L1 (1996);
 J.C. Baker *et al.*, *Monthly Not. Royal Astron. Soc.* **308**, 1173 (1999).
6. **COBE:** G. Hinshaw *et al.*, *Astrophys. J.* **464**, L17 (1996).
7. **FIRS:** K. Ganga, L. Page, E. Cheng, and S. Meyers, *Astrophys. J.* **432**, L15 (1993).
8. **IAB:** L. Piccirillo and P. Calisse, *Astrophys. J.* **413**, 529 (1993).
9. **IAC:** S.R. Dicker *et al.*, *Monthly Not. Royal Astron. Soc.*, in press, astro-ph/9907118.
10. **MAT:** E. Torbet *et al.*, *Astrophys. J.* **521**, L79 (1999);
 A.D. Miller *et al.*, *Astrophys. J.* **524**, L1 (1999).
11. **MAX:** S.T. Tanaka *et al.*, *Astrophys. J.* **468**, L81 (1996);
 M. Lim *et al.*, *Astrophys. J.* **469**, L69 (1996).

14 19. *Cosmic background radiation*

12. **MSAM:** G.W. Wilson *et al.*, *Astrophys. J.*, in press, astro-ph/9902047.
13. **OVRO:** A.C.S. Readhead *et al.*, *Astrophys. J.* **346**, 566 (1989);
E. Leitch, A.C.S. Readhead, T.J. Pearson, S.T. Myers, and S. Gulbis, *Astrophys. J.*,
in press, astro-ph/9807312.
14. **Python.:** S.R. Platt *et al.*, *Astrophys. J.* **475**, L1 (1997);
K. Coble *et al.*, *Astrophys. J.* **519**, L5 (1999).
15. **QMAP:** A. de Oliveira-Costa *et al.*, *Astrophys. J.* **509**, L77 (1998).
16. **Saskatoon:** C.B. Netterfield *et al.*, *Astrophys. J.* **474**, 47 (1997).
17. **SP91:** J. Schuster *et al.*, *Astrophys. J.* **412**, L47 (1993).
18. **SP94:** J.O. Gundersen *et al.*, *Astrophys. J.* **443**, L57 (1994).
19. **SuZIE:** S. E. Church *et al.*, *Astrophys. J.* **484**, 523 (1997).
20. **Tenerife:** C.M. Gutiérrez *et al.*, *Astrophys. J.* **529**, 47 (2000).
21. **Viper:** J.B. Peterson *et al.*, *Astrophys. J.*, in press, astro-ph/9910503.
22. **VLA:** B. Partridge *et al.*, *Astrophys. J.* **483**, 38 (1997).
23. **WD:** G.S. Tucker, G.S. Griffin, H.T. Nguyen, and J.B. Peterson, *Astrophys. J.* **419**,
L45 (1993).